

Probability density of fractional Brownian motion and the fractional Langevin equation with absorbing walls

Thomas Vojta and Alex Warhover

Department of Physics, Missouri University of Science and Technology, Rolla, MO 65409, USA

22 December 2020

Abstract. Fractional Brownian motion and the fractional Langevin equation are models of anomalous diffusion processes characterized by long-range power-law correlations in time. We employ large-scale computer simulations to study these models in two geometries, (i) the spreading of particles on a semi-infinite domain with an absorbing wall at one end and (ii) the stationary state on a finite interval with absorbing boundaries at both ends and a source in the center. We demonstrate that the probability density and other properties of the fractional Langevin equation can be mapped onto the corresponding quantities of fractional Brownian motion driven by the same noise if the anomalous diffusion exponent α is replaced by $2 - \alpha$. In contrast, the properties of fractional Brownian motion and the fractional Langevin equation with *reflecting* boundaries were recently shown to differ from each other qualitatively. Specifically, we find that the probability density close to an absorbing wall behaves as $P(x) \sim x^\kappa$ with the distance x from the wall in the long-time limit. In the case of fractional Brownian motion, κ varies with the anomalous diffusion exponent α as $\kappa = 2/\alpha - 1$, as was conjectured previously. We also compare our simulation results to a perturbative analytical approach to fractional Brownian motion.

Keywords: Anomalous diffusion, fractional Brownian motion

Contents

1	Introduction	2
2	Fractional Brownian motion	4
2.1	Definition	4
2.2	Simulation details	5
3	Fractional Langevin equation	6
3.1	Definition	6
3.2	Simulation method	7
3.3	Antipersistent noise	9

4	Normal diffusion with absorbing walls	10
5	Simulation results for FBM with absorbing walls	10
5.1	Semi-infinite interval	10
5.2	Stationary state on finite interval	15
6	Simulation results for the FLE with absorbing walls	17
6.1	Semi-infinite interval	18
6.2	Stationary state on finite interval	20
7	Conclusions	23
8	Acknowledgments	25

1. Introduction

Within the stochastic approach spearheaded by Einstein [1], Smoluchowski [2], and Langevin [3], diffusion is commonly understood as random motion. If this motion is local in time and space in the sense that (i) it features a finite correlation time after which individual steps become statistically independent, and (ii) the displacements over a correlation time feature a finite second moment, the central limit theorem applies to the sequence of random steps. This leads to the well-known linear relation $\langle x^2 \rangle \sim t$ between the mean-square displacement of the moving particle and the elapsed time t that characterizes normal diffusion [4].

Anomalous diffusion, i.e., random motion whose mean-square displacement does not obey the linear $\langle x^2 \rangle \sim t$ relation, has attracted considerable attention in recent years (for reviews see, e.g., Refs. [5–10] and references therein), partially because novel microscopic techniques provide access to the trajectories of single molecules in complex environments [11–13]. Anomalous diffusion can be caused by various mechanisms that violate the condition of locality in space and time. For example, long-range correlations in time between individual random displacements (steps) can produce subdiffusion (for which $\langle x^2 \rangle$ grows slower than t) or superdiffusion (for which $\langle x^2 \rangle$ grows faster than t) even if the step lengths and waiting times are narrowly distributed. Fractional Brownian motion (FBM) and the fractional Langevin equation (FLE) are two paradigmatic mathematical models for stochastic processes with long-time correlations.

FBM is a non-Markovian self-similar Gaussian stochastic process with stationary power-law correlated increments. Its mean-square displacement fulfills the relation $\langle x^2 \rangle \sim t^\alpha$ where α is the anomalous diffusion exponent.[‡] If the increments are positively correlated (persistent), the resulting motion is superdiffusive ($\alpha > 1$) whereas anticorrelated (antipersistent) increments produce subdiffusive motion ($\alpha < 1$). FBM has been employed to model a variety of system ranging from diffusion inside biological cells [14–19], the dynamics of polymers [20, 21], electronic network traffic [22], and

[‡] In the mathematical literature, the Hurst exponent $H = \alpha/2$ is often used instead of α .

the geometry of serotonergic fibers in vertebrate brains [23], to fluctuations of financial markets [24, 25]. FBM was put forward by Kolmogorov [26] as well as Mandelbrot and van Ness [27]. It has received attention in the mathematical literature (see, e.g., Refs. [28–31]) but only limited results are available for FBM in confined geometries because the method of images [32], typically used for Brownian motion, fails and a generalized diffusion equation for FBM has not yet been found. Available results include the solution of the first-passage problem on a semi-infinite interval [33–36]), a conjecture for a two-dimensional wedge domain [37], and results for parabolic domains [38].

FBM can be understood as random motion governed by *external* noise [39]. It does not obey the fluctuation-dissipation theorem [40] and generally does not reach a thermal equilibrium state. To describe anomalous diffusion in thermal equilibrium, one can use the fractional Langevin equation [41], a generalization of the well-know Langevin equation [3] involving a long-range correlated random force and a non-local damping force that fulfill the fluctuation-dissipation theorem [40].

Recent computer simulations of FBM with reflecting walls have shown that the interplay between the long-time correlations and the geometric confinement affects the probability density function $P(x, t)$ of the diffusing particle, and leads to strong accumulation and depletion effects. If the motion is restricted to a one-dimensional semi-infinite interval by a reflecting wall at the origin, the probability density develops a power-law singularity, $P \sim x^\kappa$ at the wall [42, 43]. The exponent κ was conjectured to depend on the anomalous diffusion exponent via $\kappa = 2/\alpha - 2$. Particles accumulate at the wall, $\kappa < 0$ for persistent noise but are depleted close to the wall, $\kappa > 0$ for anti-persistent noise. Similarly, simulations of FBM on a finite interval with reflecting walls at both ends, have shown that the stationary probability density reached for long times is nonuniform [44, 45], whereas the corresponding distribution for normal diffusion would be uniform. Simulations in higher dimensions [45] demonstrate analogous behavior. In contrast, the FLE with reflecting walls features weaker accumulation and depletion effects [46]. The stationary distribution of the FLE on a finite interval is, in fact, completely uniform independent of the value of α , as required in thermal equilibrium. Some accumulation or depletion of particles (compared to normal diffusion) does occur in nonequilibrium situations such as the motion on a semi-infinite interval. However, it is less pronounced than in the FBM case.

It is therefore interesting to compare the probability densities of FBM and the FLE in the presence of absorbing (rather than reflecting) boundary conditions. The purpose of the present paper is to explore this question systematically by means of large-scale computer simulations. For the case of FBM, important results have already been obtained in the literature [47]. Specifically, the probability density close to an absorbing wall has been conjectured to vanish as $P(x) \sim x^\kappa$ with exponent $\kappa = 2/\alpha - 1$ with the distance x from the wall [48]. A perturbative expansion about the normal diffusion case agrees with this conjecture to first order in $\alpha - 1$ [49]. This perturbative approach was later employed to compute not just exponents but complete scaling functions of various FBM observables [50–52].

In the present paper, we focus on comparing the probability densities of the FLE and FBM in the presence of absorbing walls. We consider two geometries, (i) a semi-infinite interval having an absorbing wall at the origin and (ii) a finite interval with absorbing boundaries at both ends and a source in the center. Our paper is organized as follows. FBM and the FLE are introduced in Secs. 2 and 3, respectively, where we also outline our numerical approaches. For comparison purposes, Sec. 4 summarizes the behavior of normal diffusion with absorbing walls. The simulation results for FBM with absorbing walls are given in Sec. 5. Section 6 presents the corresponding results for the FLE together with comparison between the two stochastic processes. We conclude in Sec. 7.

2. Fractional Brownian motion

2.1. Definition

Unconfined FBM is a non-Markovian continuous-time Gaussian stochastic process with stationary increments. It is centered, i.e., the average of the position X at time t vanishes, $\langle X(t) \rangle = 0$. The position covariance function reads

$$\langle X(s)X(t) \rangle = K(s^\alpha - |s - t|^\alpha + t^\alpha) \quad (1)$$

The exponent α can take values in the range $0 < \alpha < 2$. The mean-square displacement of the process is obtained from eq. (1) by setting $s = t$, resulting in anomalous diffusion $\langle X^2 \rangle = 2Kt^\alpha$, i.e., superdiffusion for $\alpha > 1$ and subdiffusion for $\alpha < 1$. The marginal case $\alpha = 1$ corresponds to normal diffusion. The increment process $\xi(t)$ defined via

$$X(t) = \int_0^t dt' \xi(t') \quad (2)$$

constitutes a fractional Gaussian noise [53], i.e., a stationary Gaussian process of zero mean and covariance

$$\langle \xi(t)\xi(t') \rangle = K\alpha(\alpha - 1)|t - t'|^{\alpha-2} \quad (t \neq t'). \quad (3)$$

The correlations are positive (persistent) for $\alpha > 1$ and negative (anti-persistent) for $\alpha < 1$. In the marginal case, $\alpha = 1$, the covariance vanishes for all $t \neq t'$. The probability density of unconfined FBM takes the Gaussian form

$$P(x, t) = \frac{1}{\sqrt{4\pi Kt^\alpha}} \exp\left(-\frac{x^2}{4Kt^\alpha}\right). \quad (4)$$

In preparation for the computer simulations, we now discretize time using a time step ϵ by setting $t_n = \epsilon n$ (where n is an integer) and $x_n = X(t_n)$. The resulting discrete version of FBM [53] can be understood as a random walk with identically Gaussian distributed but long-time correlated increments. Specifically, the position x_n of the particle follows the recursion relation

$$x_{n+1} = x_n + \xi_n. \quad (5)$$

The increments ξ_n are Gaussian random numbers of zero mean, variance $\sigma^2 = 2K\epsilon^\alpha$, and covariance function

$$C_n = \langle \xi_m \xi_{m+n} \rangle = \frac{1}{2} \sigma^2 (|n+1|^\alpha - 2|n|^\alpha + |n-1|^\alpha). \quad (6)$$

In the long-time limit $n \rightarrow \infty$, this covariance takes the power-law form $\langle \xi_m \xi_{m+n} \rangle \sim \alpha(\alpha-1)|n|^{\alpha-2}$, in agreement with the continuum version (3).

To approximate the continuum limit, the time step ϵ of the discrete FBM must be much smaller than the considered total times t . Equivalently, the standard deviation σ of an individual increment must be small compared to typical distances or system sizes. This can be achieved either by taking ϵ to zero at fixed t or, equivalently, by taking t to infinity at fixed ϵ .

Absorbing walls can be easily implemented by suitably modifying the recursion relation (5). As the fractional Gaussian noise is understood as externally given [39], it is not affected by the walls. Specifically, an absorbing wall at position w that confines the particles to $x \geq w$ (i.e., a wall to the left of the allowed interval) can be defined by simply removing the particle whenever $x_n < w$. A wall confining the motion to positions $x \leq w$ (i.e., a wall at the right end of an allowed interval) can be defined analogously. We note in passing that the definition of *reflecting* walls is not as straight forward because there is some ambiguity in where to place the particle after the interaction with the wall. For a discussion of this issue see, e.g., Ref. [45] and references therein.

2.2. Simulation details

We perform extensive computer simulations of the discrete-time FBM defined by eqs. (5) and (6) for several anomalous diffusion exponents α between 0.6 (subdiffusive regime) and 1.6 (superdiffusive regime). We set the time step to $\epsilon = 1$ and fix K at $K = 1/2$. The resulting standard deviation of the individual increments ξ_n is $\sigma = 1$.

We consider two geometries. In the first set of simulations, the particles start at position x_0 and are confined to nonnegative x values by an absorbing wall at the origin, $x = 0$. The maximum time ranges from $2^{17} \approx 130,000$ deep in the superdiffusive regime ($\alpha = 1.6$) to $2^{23} \approx 8.4$ million for the most subdiffusive $\alpha = 0.6$. These long times allow us to reach the continuum (scaling) limit for which the time discretization becomes unimportant. Because a significant fraction of the particles is absorbed by the absorbing wall before the final time, these simulations require large numbers of particles. We start the simulations with 10^8 to 10^9 particles to reach a statistical accuracy that allows us to analyze the probability density at the final time.

In the second set of simulations, the particles start at the origin and are confined to the finite interval $[-L/2, L/2]$ by absorbing walls at both ends. If a particle is absorbed by one of the walls, it is not removed but placed back at the origin (and the memory of its previous steps is erased). This models a particle source at the center of the interval. In these simulations, we focus on the steady state that is reached after sufficiently long times. It is characterized by a constant particle current from the center of the interval

to the absorbing walls. We employ interval length ranging from $L = 4 \times 10^5$ for $\alpha = 1.6$ to $L = 400$ for $\alpha = 0.6$. All lengths fulfill the condition $L/\sigma \gg 1$ necessary to reach the continuum (scaling) limit for the discrete FBM. As no particles are lost in these simulations, they require smaller particle numbers. We use between 10^4 and 5×10^4 particles for each simulation run. The longest times reached for each α are in the range from $2^{25} \approx 33$ million to $2^{27} \approx 134$ million.

The correlated Gaussian random numbers ξ_n that represent the discrete fractional Gaussian noise (the FBM increments or steps) are precalculated before each particle performs the random walk. (If a particle is placed back at the origin after absorption in the second set of simulations, its set of random numbers is discarded, and a new set of random numbers is created.) The random numbers are created by means of the Fourier-filtering technique [54] which consists of the following steps: First, a sequence of independent Gaussian random numbers χ_i of zero average and unit variance is created (using the Box-Muller transformation with the LFSR113 random number generator proposed by L'Ecuyer [55] as well as the 2005 version of Marsaglia's KISS [56]). The discrete Fourier transform $\tilde{\chi}_\omega$ of these numbers is then converted via $\tilde{\xi}_\omega = [\tilde{C}(\omega)]^{1/2} \tilde{\chi}_\omega$, where $\tilde{C}(\omega)$ is the Fourier transform of the covariance function (6) of the fractional Gaussian noise. The desired correlated noise values ξ_n are given by the inverse Fourier transformation of the $\tilde{\xi}_\omega$.

The computational effort of the Fourier-filtering technique scales as $N_t \ln N_t$ with the number of time steps while the effort for the actual propagation of the recursion relation (5) scales linearly with N_t . Overall, our simulations thus show a favorable, almost linear scaling with N_t . This allows us to reach long times and employ large numbers of particles.

3. Fractional Langevin equation

3.1. Definition

The well-known normal Langevin equation [3],

$$m \frac{d^2}{dt^2} x(t) = -\bar{\gamma} \frac{d}{dt} x(t) + \xi_w(t) , \quad (7)$$

describes the motion of a particle of mass m under the influence of an uncorrelated random force (Gaussian white noise) $\xi_w(t)$ and a linear instantaneous damping force with damping coefficient $\bar{\gamma}$.

The Langevin equation can be generalized [57–59] by considering a correlated random force $\xi(t)$ and a nonlocal (in time) damping force, leading to the equation

$$m \frac{d^2}{dt^2} x(t) = -\bar{\gamma} \int_0^t dt' \mathcal{K}(t-t') \frac{d}{dt'} x(t') + \xi(t) . \quad (8)$$

If the noise covariance and the damping (memory) kernel \mathcal{K} fulfill the relation

$$\langle \xi(t) \xi(t') \rangle = k_B T \bar{\gamma} \mathcal{K}(t-t') , \quad (9)$$

the fluctuation-dissipation theorem [40] guarantees that the system reaches thermal equilibrium at temperature T in the long-time limit. If the random force is a fractional Gaussian noise (as introduced in Sec. 2.1), i.e., a stationary Gaussian process of zero mean and covariance (3), the equation is called the fractional Langevin equation (FLE). Note that the exponent α in the fractional Gaussian noise is restricted to the range $1 < \alpha < 2$ because the damping integral in (8) diverges at $t = t'$ for $\alpha < 1$, and $\alpha > 2$ is unphysical because it implies correlations that increase with time.

The properties of the unconfined (free-space) FLE are well understood (see, e.g., Ref. [8] and references therein). If the particle starts from rest at the origin at time $t = 0$, the probability densities of both its velocity and its position are Gaussians of zero mean. In the long-time limit, the mean-square velocity reaches the equilibrium value $k_B T/m$ required by the equipartition theorem. The mean-square displacement initially shows ballistic behavior, $\langle x^2(t) \rangle \sim t^2$, and then crosses over to anomalous diffusion,

$$\langle x^2(t) \rangle \sim t^{2-\alpha} , \quad (10)$$

at longer times. This means the anomalous diffusion exponent of the FLE is actually $2 - \alpha$ rather than α as it was for FBM. It also implies that the FLE with persistent noise, $1 < \alpha < 2$, leads to subdiffusion while FBM with the same noise produces superdiffusion. This difference between FBM and the FLE stems from the fact that the fluctuation-dissipation condition (9) combines persistent noise with long-time memory in the damping force.

Absorbing walls can be introduced in complete analogy to FBM in Sec. 2.1. An absorbing wall at position w that confines the particles to $x \geq w$ is defined by simply removing the particle whenever $x(t) < w$. A wall confining the motion to positions $x \leq w$ is defined analogously. §

3.2. Simulation method

Our computer simulations of the FLE follow the efficient approach detailed in Ref. [46]. In the present section, we provide a brief outline of the method.

We start by discretizing the time variable, $t_n = \epsilon n$ (where n is an integer) and replacing the time derivatives in the FLE by first-order finite-difference expressions. This yields the recursion relations

$$v_{n+1} = v_n + \epsilon \left[\xi_n - \sum_{m=0}^n \mathcal{K}_{n-m} v_m \right] , \quad (11)$$

$$x_{n+1} = x_n + \epsilon v_n \quad (12)$$

which are easily propagated numerically. The ξ_n are a discrete fractional Gaussian noise [53], i.e., identical Gaussian random numbers of zero mean and covariance (6), and we have fixed the mass m , the damping coefficient $\bar{\gamma}$, and the Boltzmann constant k_B at

§ As in the FBM case, *reflecting* walls pose additional challenges; this has been discussed, e.g., in Ref. [46].

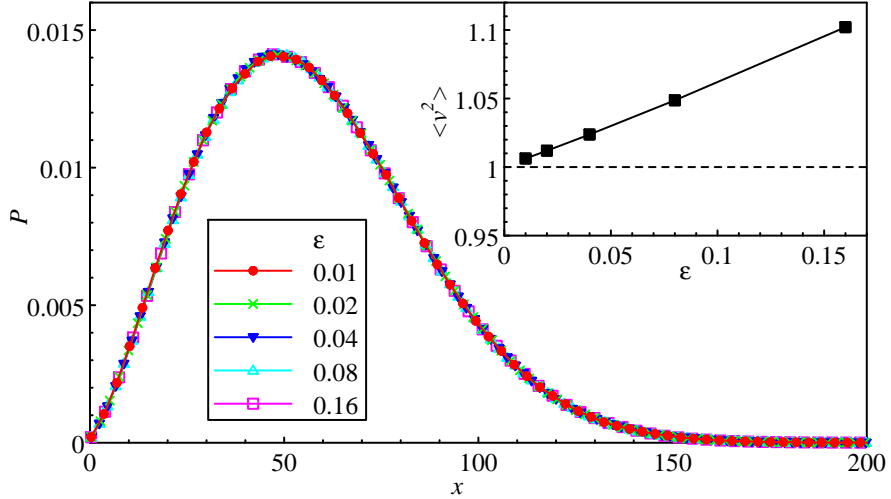


Figure 1. Determination of a suitable value of the time step ϵ . Main panel: probability density $P(x, t)$ of the particle position at time $t = 5234$ for correlation exponent $\alpha = 1.2$, temperature $T = 1$, and several values of the time step ϵ . The particles start $x_0 = 10$ at time $t = 0$ and move on the semi-infinite interval $(0, \infty)$ with an absorbing wall at the origin. Inset: Stationary mean-square velocity $\langle v^2 \rangle$ as a function of time step ϵ (the data are averages of $\langle v^2 \rangle$ over the surviving particles during the time intervals 1000 – 5000). The statistical error is smaller than the symbol size.

unity. The damping kernel fulfills the discrete version of the fluctuation-dissipation theorem,

$$TK_n = \langle \xi_m \xi_{m+n} \rangle. \quad (13)$$

The numerical effort for creating the correlated random forces by means of the Fourier filtering method scales as $N_t \ln N_t$ with the number of time steps, as explained in Sec. 2.2. However, a naive implementation of the recursion relation (11) leads to an unfavorable quadratic scaling of the effort with N_t because the damping sum contains $O(N_t)$ terms for every single time step. We have therefore developed an improved algorithm that speeds up the evaluation of the damping integrals by several orders of magnitude. It is based on the fact that the damping kernel is small and slowly varying for large time lag $n - m$ and effectively reduces the scaling of the numerical effort from N_t^2 to $N_t^{1.2}$, albeit with a large prefactor. This algorithm is discussed in detail in the Appendix of Ref. [46].

The performance of the simulations depends on choosing a suitable value for the time step ϵ . On the one hand, ϵ should be small to reduce the time discretization error. On the other hand, a small ϵ increases the numerical effort to reach long times. To optimize the time step, we study how the stationary value of the mean-square velocity $\langle v^2 \rangle$ depends on the time step. Results for particles moving on the semi-infinite interval $[0, \infty)$ are shown in the inset of Fig. 1. The data indicate that the deviation of $\langle v^2 \rangle$ from the value of 1 (required by the fluctuation-dissipation theorem for temperature $T = 1$) decreases with decreasing ϵ , as expected. The relative error is below 5% for

times steps $\epsilon = 0.08$ and smaller. We also test how the probability density $P(x, t)$ is affected by the time step ϵ . The main panel of Fig. 1 presents results for $\alpha = 1.2$ and $t = 5243$. They show that the probability densities for time steps between $\Delta t = 0.01$ and 0.16 fall right on top of each other. In the majority of our simulations, we therefore employ time steps $\epsilon = 0.04$ and 0.08.

All simulations are performed for noise amplitude $K = 1$ and temperature $T = 1$, using the same two geometries as for FBM. In a first set of calculations, particles start at a position $x_0 > 0$ and are confined to the nonnegative x axis by an absorbing wall at $x = 0$. The longest simulations use 2^{25} time steps of size $\epsilon = 0.08$ giving a maximum time of about 2.7×10^6 . The initial particle number is between 10^7 and 5×10^8 . In the second set of calculations, particles start at the origin and are confined to the interval $[-L/2, L/2]$ by absorbing walls at both ends. When a particle is absorbed by one of the walls, it is placed back at the origin. We consider two restart conditions, (i) the particle retains its random force sequence and velocity memory or (ii) the particle restarts with a fresh set of random forces and has no memory of its velocities before the absorption. Condition (ii) is perhaps more physically plausible and corresponds to the method used for FBM. Most of our simulations thus employ condition (ii), but we also carry out a few test calculations using condition (i). The two cases are expected to produce slightly different steady states, but with the same qualitative behavior close to the absorbing walls. We use up to 2^{29} time steps and employ interval length between 400 and 10^5 , depending on α . As no particles are lost in these simulations, they require smaller particle numbers. We use between 5000 and 20000 particles for each run.

3.3. Antipersistent noise

In the continuous-time FLE (8), the exponent α of the random force is restricted to $1 < \alpha < 2$, i.e., to the case of persistent noise. Anti-persistent noise, $\alpha < 1$ is impossible because the damping integral diverges in this case. Because the divergence stems from short time lags near $t = t'$, it can be cut off without modifying the physically important long-time behavior of the the damping kernel. In the discretized FLE defined via eqs. (11) and (12) the singularity is already cut off as the damping sum in (11) remains finite for all correlation exponents in the full interval $0 < \alpha < 2$. This allows us to extend our simulation to the anti-persistent case.

The behavior of the discretized FLE in the regime $\alpha < 1$ is rather peculiar. The (discrete) fluctuation-dissipation theorem (13) implies that the damping kernel \mathcal{K}_{n-m} has negative values for $n \neq m$ if the noise is antipersistent. Instead of damping, these terms thus yield antidamping, i.e., a positive feedback for the velocity. Consequently, the mean-square displacement for the free, unconfined FLE, $\langle x^2 \rangle \sim t^{2-\alpha}$, grows super-diffusively for $\alpha < 1$.

4. Normal diffusion with absorbing walls

For comparison purposes, this section briefly summarizes the relevant results for normal diffusion. In this case, the probability density $P(x, t)$ can be found by solving the diffusion equation $\partial_t P(x, t) = K \partial_{xx} P(x, t)$.

In our first geometry, all particles start at $x_0 > 0$ at time $t = 0$, and are confined to the non-negative x -axis by an absorbing wall at the origin, $x = 0$. The diffusion equation thus has the initial condition $P(x, 0) = \delta(x - x_0)$ and the absorbing boundary condition $P(0, t) = 0$. This problem can be solved easily by means of the method of images [32], giving

$$P(x, t) = \frac{1}{\sqrt{4\pi Kt}} \left[\exp\left(-\frac{(x - x_0)^2}{4Kt}\right) - \exp\left(-\frac{(x + x_0)^2}{4Kt}\right) \right]. \quad (14)$$

Integrating $P(x, t)$ over all $x \geq 0$ yields the survival probability

$$S(t) = \frac{1}{\sqrt{4\pi Kt}} \int_{-x_0}^{x_0} dx \exp\left(-\frac{x^2}{4Kt}\right) \rightarrow \begin{cases} 1 & \text{if } 2Kt \ll x_0^2 \\ x_0/\sqrt{\pi Kt} & \text{if } 2Kt \gg x_0^2 \end{cases}. \quad (15)$$

The conditional probability density $P_s(x, t) = P(x, t)/S(t)$ for the surviving particles takes the form

$$P_s(x, t) = \frac{x}{2Kt} \exp\left(-\frac{x^2}{4Kt}\right) \quad (16)$$

in the long time limit $2Kt \gg x_0^2$. The corresponding mean square displacement of the surviving particles from the origin reads $\langle x^2 \rangle = 4Kt$ (twice the value of free Brownian motion).

In our second geometry, we consider the steady state on a finite interval $[-L/2, L/2]$ with absorbing walls at both ends and a source in the center. The stationary solution of the diffusion equation with boundary conditions $P(-L/2, t) = P(L/2, t) = 0$ reads

$$P(x, t) = \frac{2}{L} \left(1 - \frac{2|x|}{L}\right), \quad (17)$$

when it is properly normalized to unity.

5. Simulation results for FBM with absorbing walls

5.1. Semi-infinite interval

In this section, we report the results of FBM simulations in which the particles start at a position $x_0 > 0$ at time $t = 0$ and are confined to the semi-infinite interval $[0, \infty)$ by an absorbing wall at the origin. Figure 2 gives an overview over the time evolution of the survival probability $S(t)$ and mean-square displacement $\langle x^2 \rangle$ from the origin of the surviving particles for $x_0 = 10$ and several values of the anomalous diffusion exponent α that cover the range from subdiffusive to superdiffusive behavior. The long-time decay

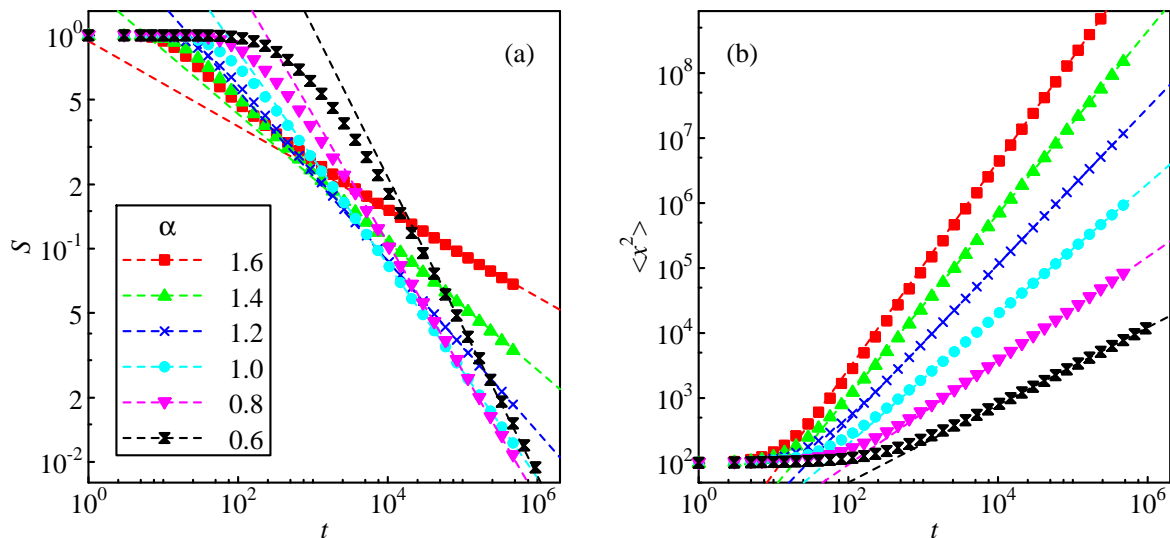


Figure 2. FBM on the semi-infinite interval $[0, \infty)$. (a) Survival probability S vs. time t for several values of α . The initial particle number ranges from 10^7 to 10^8 , all particles start at $x_0 = 10$. The dashed lines are fits of the long-time behavior to the expected power law $S(t) \sim t^{-(1-\alpha/2)}$. (b) Mean square displacement from the origin $\langle x^2 \rangle$ of the surviving particles vs. time t for the same simulations as in panel (a). The dashed lines are fits of the long-time behavior to the expected power law $\langle x^2 \rangle \sim t^\alpha$. The statistical errors of all data points are smaller than the symbol size.

of the survival probability is expected to follow the power-law $S(t) \sim t^{-\theta}$ with θ being the persistence exponent, which is known exactly for FBM, $\theta = 1 - \alpha/2$ [35, 48]. The data in Fig. 2(a) agree very well with this power law for all studied values of α . The mean-square displacement from the origin for the surviving particles, shown in Fig. 2(b) follows the same anomalous diffusion power law, $\langle x^2 \rangle \sim t^\alpha$, as it would for free FBM. We also note that, for normal Brownian motion $\alpha = 1$, the prefactors of both power laws agree with the diffusion equation results of Sec. 4 with high accuracy. Simulations starting from different initial positions x_0 lead to analogous results. In fact, the survival probability curves for different x_0 collapse onto each other when plotted as a function of $t/x_0^{2/\alpha}$ implying the scaling from $S(t, x_0) = F(t/x_0^{2/\alpha})$. The mean-square displacement of the *surviving* particles becomes independent of x_0 for sufficiently long times.

We now turn to the time evolution of the probability density $P(x, t)$, starting from the initial condition $P(x, 0) = \delta(x - x_0)$. We mostly discuss the conditional probability density $P_s(x, t) = P(x, t)/S(t)$ for the surviving particles, which is properly normalized to unity for all times.

Let us start by focusing on the value $\alpha = 1.2$ of the anomalous diffusion exponent. Figure 3 illustrates the time evolution of $P_s(x, t)$ in this case. Panel 3(a) shows that $P_s(x, t)$ follows, for early times, a Gaussian distribution centered at $x_0 = 10$ whose width grows like $t^{\alpha/2}$, just as in the case of free, unconfined FBM. Once the distribution starts interacting with the absorbing wall, the functional form of $P_s(x, t)$ changes. Whereas the

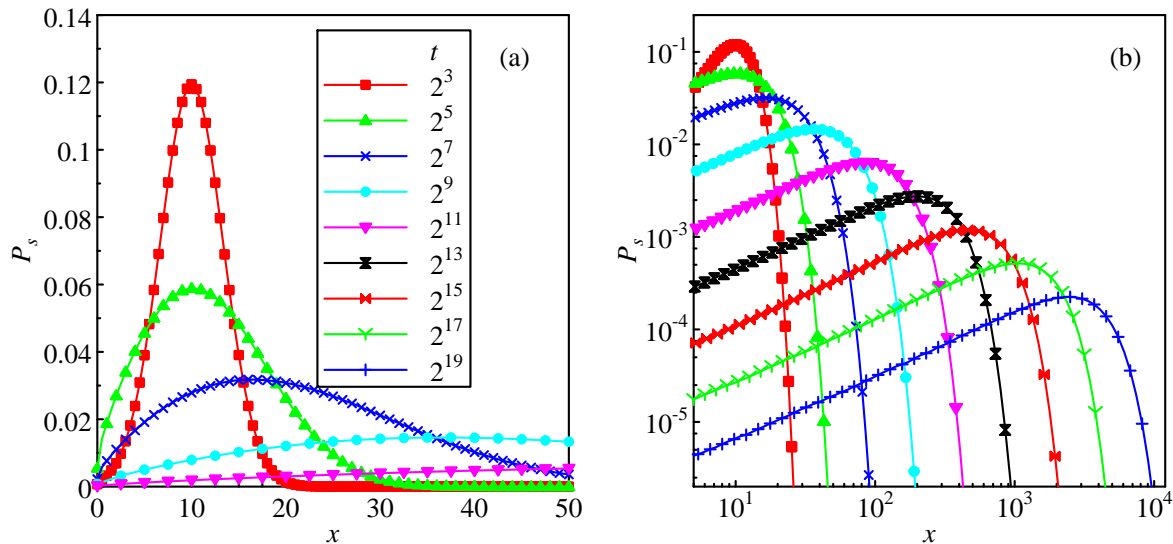


Figure 3. Time evolution of the conditional probability density $P_s(x, t)$ for FBM with anomalous diffusion exponent $\alpha = 1.2$, confined to the positive x -axis by an absorbing wall at the origin. The initial particle number is 5×10^8 , all particles start at $x_0 = 10$. To further improve the statistics, P_s is averaged over a short time interval around the given time. (a) Linear plot of P_s vs. x covering the early time behavior. (b) Double-logarithmic plot of P_s vs. x for all simulated times. The statistical errors of all data points are smaller than the symbol size.

large- x tail remains Gaussian, the behavior close to the absorbing wall takes a power-law form with an exponent that is independent of time. This is demonstrated in Fig. 3(b).

The conditional probability distributions for sufficiently long times can be collapsed onto a single master curve by plotting the distribution in terms of the reduced variables $y = x/x_m(t)$ and $Y = P_s x_m(t)$ where $x_m(t) = \langle x^2(t) \rangle^{1/2}$ is the root mean square displacement of the surviving particles from the origin. Figure 4(a) indicates a nearly perfect data collapse for times $t \geq 2^9$, about the time where the survival probability and mean-square displacement in Fig. 2 reach their asymptotic power-law behaviors. The figure also shows that the small- x data for each of the curves deviate from the common master curve. These deviations stem from the time discretization (finite time step ϵ); they occur for x of the order of the step width $\sigma = 1$. As the distribution broadens with increasing time, the onset of these time discretization artifacts is pushed to smaller y as t increases. The data collapse in Fig. 4(a) implies that the conditional probability density fulfills the scaling from

$$P_s(x, t) = \frac{1}{x_m(t)} Y_\alpha^{\text{fbm}} \left[\frac{x}{x_m(t)} \right] = \frac{1}{\sqrt{2Kt^\alpha}} \tilde{Y}_\alpha^{\text{fbm}} \left[\frac{x}{\sqrt{2Kt^\alpha}} \right] \quad (18)$$

in the long-time limit $x_m(t) \gg x_0$. Note that the analytical expression (16) for the distribution in the normal diffusion case, $\alpha = 1$, does fulfill this scaling form. Simulations starting from different initial positions x_0 reveal that the conditional probability densities become independent of x_0 for $x_m(t) \gg x_0$, implying that the scaling

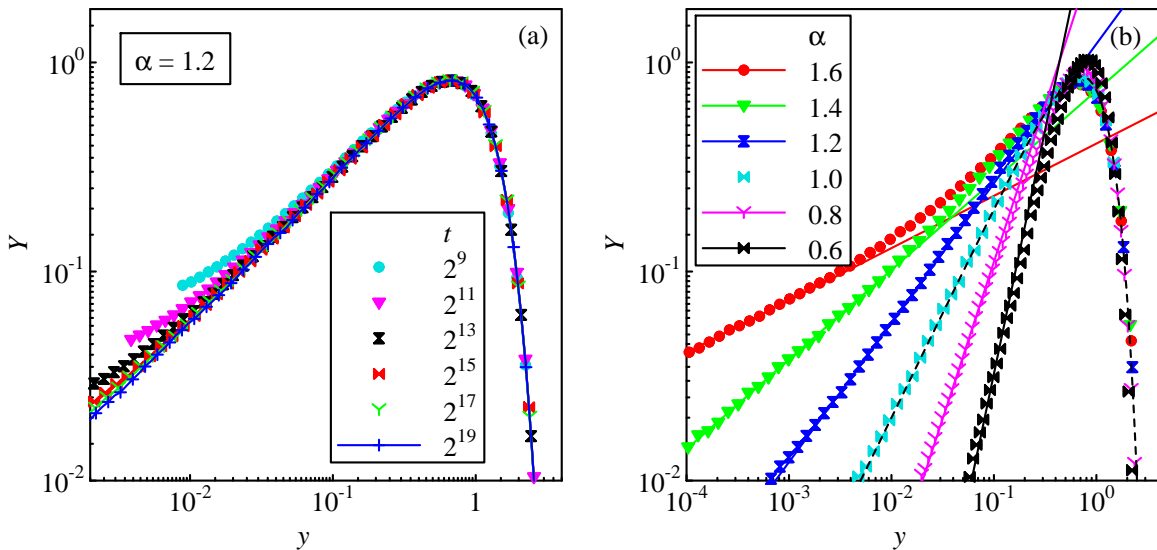


Figure 4. Conditional probability densities of FBM on the semi-infinite interval $[0, \infty)$ for $x_0 = 10$, expressed in terms of the reduced variables $y = x/x_m(t)$ and $Y = P_s x_m(t)$ with $x_m(t) = \langle x^2(t) \rangle^{1/2}$. (a) Data for $\alpha = 1.2$ at different times. The deviations from the common master curve at the smallest x for each t stem from the time discretization, they occur for x of the order of the step width $\sigma = 1$. (b) Data for different α at the longest simulated times, ranging from $t = 2^{17}$ (for $\alpha = 1.6$) to $t = 2^{23}$ (for $\alpha = 0.6$). The solid lines are fits of the small- y behavior to the conjectured power law $Y \sim y^\kappa$ with $\kappa = 2/\alpha - 1$. The dashed line corresponds to the analytical result (16) for normal diffusion, without adjustable parameters. The statistical errors of the data points are about a symbol size (for the smallest shown Y) or smaller.

function Y_α^{fbm} does not depend on x_0 .

We have performed analogous simulations for several α between 0.6 and 1.6. The resulting conditional probability densities $P_s(x, t)$ all fulfill the scaling form (18). Figure 4(b) compares $P_s(x, t)$ for all simulated α (using the data taken at the longest simulated time for each α). The data for the normal diffusion case, $\alpha = 1$, agree nearly perfectly with the analytical solution (16), without adjustable parameters. This gives us additional confidence in the precision of our simulations. All distributions show power-law behavior close to the absorbing wall, $y \ll 1$. The data in this regime can be fitted with high accuracy with the conjectured [48] power law $Y \sim y^\kappa$ with $\kappa = 2/\alpha - 1$. For our most subdiffusive simulation, $\alpha = 0.6$, some slight deviations can be observed between the conjectured power law and the numerical data (which are slightly less steep). They can be attributed to the simulations not having progressed far enough into the asymptotic long-time regime. (The power-law behavior can, at best, be expected in the x range between the step size and the root mean square displacement, $\sigma \ll x \ll x_m(t)$. For $\alpha = 0.6$, this range is very narrow, $10 \lesssim x \lesssim 20$, even at our longest simulation time $t = 2^{23}$.)

In recent years, a number of analytical results for FBM have been obtained by means of a perturbative method [49–52] in which observables are expanded about the normal

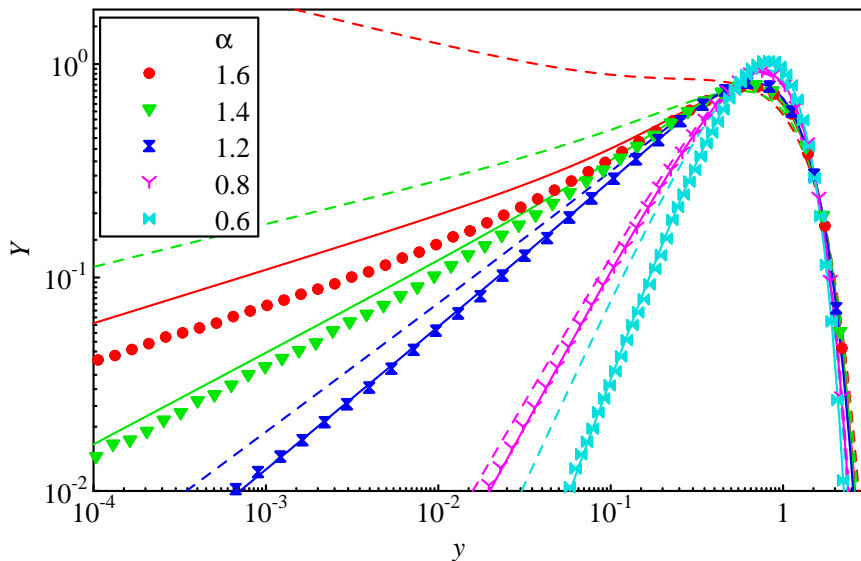


Figure 5. Comparison of the scaled conditional probability densities and the predictions of the perturbative approach in terms of the scaling variables $y = x/x_m(t)$ and $Y = P_s x_m(t)$. The symbols show our numerical data. The dashed lines correspond to the first-order expression (19) while the solid lines show the improved result (21). Note that the scaling variables y and \tilde{y} are not identical but related by a constant but α -dependent factor.

Brownian motion case, $\alpha = 1$, with $\epsilon = (\alpha - 1)/2$ being the small parameter. Within this approach, the scaling function $\tilde{Y}_\alpha^{\text{fbm}}$ of the conditional probability density $P_s(x, t)$ [defined in eq. (18)] can be written in terms of the scaling variable $\tilde{y} = x/(2Kt^\alpha)^{1/2}$ as

$$\tilde{Y}_\alpha^{\text{fbm}}(\tilde{y}) = \tilde{y} e^{-\tilde{y}^2/2} e^{\epsilon W(\tilde{y})} \quad (19)$$

to linear order in ϵ [51]. Here, the term $\tilde{y} e^{-\tilde{y}^2/2}$ represents the solution (16) for normal Brownian motion, while $e^{\epsilon W(\tilde{y})}$ encodes the perturbative correction. The function $W(\tilde{y})$ reads [49, 51]

$$\begin{aligned} W(\tilde{y}) = & \frac{1}{6} \tilde{y}^4 {}_2F_2 \left(1, 1; \frac{5}{2}, 3; \frac{\tilde{y}^2}{2} \right) + \pi(1 - \tilde{y}^2) \operatorname{erfi} \left(\frac{\tilde{y}}{\sqrt{2}} \right) + \sqrt{2\pi} e^{\tilde{y}^2/2} \tilde{y} \\ & + (\tilde{y}^2 - 2)[\gamma_E + \ln(2\tilde{y}^2)] - 3\tilde{y}^2 \end{aligned} \quad (20)$$

where ${}_2F_2$ is a hypergeometric function, erfi is the imaginary error function, and γ_E is the Euler constant. The resulting asymptotic behavior close to the wall (i.e., for $\tilde{y} \ll 1$) takes the form $\tilde{Y}_\alpha^{\text{fbm}}(\tilde{y}) \sim \tilde{y}^{1-4\epsilon} = \tilde{y}^{3-2\alpha}$. The exponent $\kappa = 1 - 4\epsilon$ agrees with the conjecture $\kappa = 2/\alpha - 1$ to linear order in ϵ . Figure 5 compares our numerical data for the conditional probability density with the analytical result (19). The figure shows that eq. (19) describes the bulk of the distributions reasonably well even for α -values far away from $\alpha = 1$. However, the power-law behavior close to the wall is not reproduced correctly because the first-order approximation of κ differs from the (conjectured) exact value. By combining the conjectured exact power law $\tilde{Y}_\alpha^{\text{fbm}}(\tilde{y}) \sim \tilde{y}^{2/\alpha-1}$ with the first-

order expression (19), one can write down an improved approximation [51],

$$\tilde{Y}_\alpha^{\text{fbm}}(\tilde{y}) = \tilde{y}^{2/\alpha-1} e^{-\tilde{y}^2/2} e^{\epsilon[W(\tilde{y})+4\ln(\tilde{y})+\text{const}]} . \quad (21)$$

The expressions (19) and (21) agree with each other to linear order in ϵ but (21) captures the exact asymptotic power law close to the wall. Figure 5 shows that eq. (21) provides a nearly perfect description of the entire distribution for a sizable α range around $\alpha = 1$. Moreover, it remains a good approximation even for α further away from unity.

The simulation of FBM confined to the semi-infinite interval $[0, \infty)$ by an absorbing wall at the origin is numerically very expensive. On the one hand, long simulation runs are necessary to reach the asymptotic long-time regime characterized by $x_m(t) \gg x_0$ and $x_m(t) \gg \sigma$. On the other hand, the survival probability $S(t)$ drops rapidly with increasing time, requiring large initial particle numbers in order to keep the statistical error at late times under control. In the next section, we therefore perform simulations that avoid the particle loss.

5.2. Stationary state on finite interval

In this section, we consider FBM on the finite interval $[-L/2, L/2]$ with absorbing walls at both ends. Particles start at the origin at $t = 0$. When a particle is absorbed by one of the walls, it is placed back at the origin and the memory of its previous motion is erased. (This is achieved by creating a new set of random displacements, completely independent of those before the absorption event.) This procedure models a particle source at the center of the interval that releases particles at the same rate as they are absorbed by the walls. The number of particles in these simulations consequently does not decrease with time. Thus, fewer (initial) particles than in the semi-infinite interval simulations are sufficient to control the statistical error, allowing us to reach longer times, up to $t = 2^{27}$.

Figure 6 gives an overview over these simulations. Panel (a) presents the time dependence of the mean-square displacement for several α . It initially follows the same anomalous diffusion behavior, $\langle x^2 \rangle \sim t^\alpha$ as free, unconfined FBM. Once the particles reach the wall, $\langle x^2 \rangle$ crosses over to a constant value that varies with α , indicating that the steady-state distribution of the particles itself is α dependent. In the continuum limit $L \gg \sigma$, the stationary mean-square displacement is proportional to L^2 . [This also follows from the scaling law (22) discussed below.] The relation between the stationary value of $\langle x^2 \rangle / L^2$ and α is detailed in the inset of Fig. 6(a). In the normal diffusion case, $\alpha = 1$, our result agrees with the value $\langle x^2 \rangle = L^2/24$ that follows from the analytical solution (17). For $\alpha \rightarrow 2$, the stationary value of $\langle x^2 \rangle$ approaches $L^2/12$. This corresponds to the flat distribution expected for ballistic motion from the source towards the absorbing walls. For $\alpha \rightarrow 0$, the stationary $\langle x^2 \rangle$ approaches zero, as expected.

Figure 6(b) illustrates the time evolution of the probability density for $\alpha = 1.2$. Initially, $P(x, t)$ features the same Gaussian shape as it would for free FBM. Once particles reach the wall, the shape of $P(x, t)$ changes. For long times (larger than about 2^{21} in this example), $P(x, t)$ become stationary and time-independent.

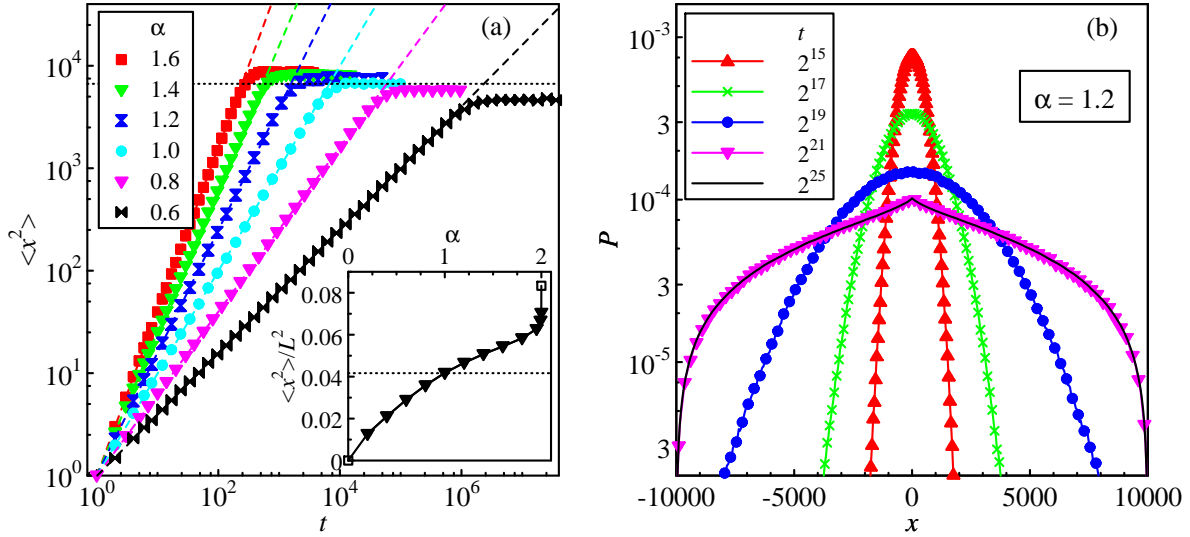


Figure 6. FBM on a finite interval $[-L/2, L/2]$ with absorbing walls at both ends and a source in the center. (a) Mean square displacement $\langle x^2 \rangle$ vs. time t for interval length $L = 400$ and several α . The data are averages over 10,000 to 20,000 particles. The dashed lines are fits to the anomalous diffusion power law $\langle x^2 \rangle \sim t^\alpha$. The dotted line marks the stationary value $\langle x^2 \rangle = L^2/24$ that follows from eq. (17) for normal diffusion. Inset: Saturation value of $\langle x^2 \rangle/L^2$ vs. α . The open squares mark the values $L^2/12$ and 0 expected for $\alpha = 2$ and 0, respectively. (b) Time evolution of the probability density $P(x, t)$ for interval length $L = 20,000$ and $\alpha = 1.2$ (between 5×10^4 and 4×10^6 particles used). All statistical errors are smaller than the symbol size.

It is interesting to compare the stationary probability densities P_{st} for several interval lengths L . Figure 7(a) presents the corresponding simulation data for several L between 100 and 80000 using scaled variables LP_{st} vs. x/L . The curves for different L collapse nearly perfectly onto a common master curve, demonstrating that the stationary distribution fulfills the scaling form

$$P_{st}(x, L) = \frac{1}{L} Z_\alpha^{\text{fbm}} \left(\frac{x}{L} \right), \quad (22)$$

where $Z_\alpha^{\text{fbm}}(z)$ is a dimensionless scaling function. Small deviations can be attributed to finite-size and finite-time effects that vanish in the limits $L \gg \sigma$, $2Kt^\alpha \gg L^2$. We have performed analogous simulations for other values of the anomalous diffusion exponent α . Figure 7(b) focuses on the behavior of the (scaled) stationary distribution near the absorbing wall located at $w = -L/2$ for several α . Sufficiently close to the wall, all probability densities follow power laws in the distance from the wall. They can be fitted with high accuracy with $P_{st}(x) \sim (x-w)^\kappa$ with $\kappa = 2/\alpha - 1$, i.e., with the same exponent as observed in the simulations on the semi-infinite interval. In addition, we have also analyzed the stationary probability density close to the particle source in the center of the interval. This analysis is somewhat more complicated than that near the absorbing walls because the value of probability density at $x = 0$ is an additional fitting parameter.

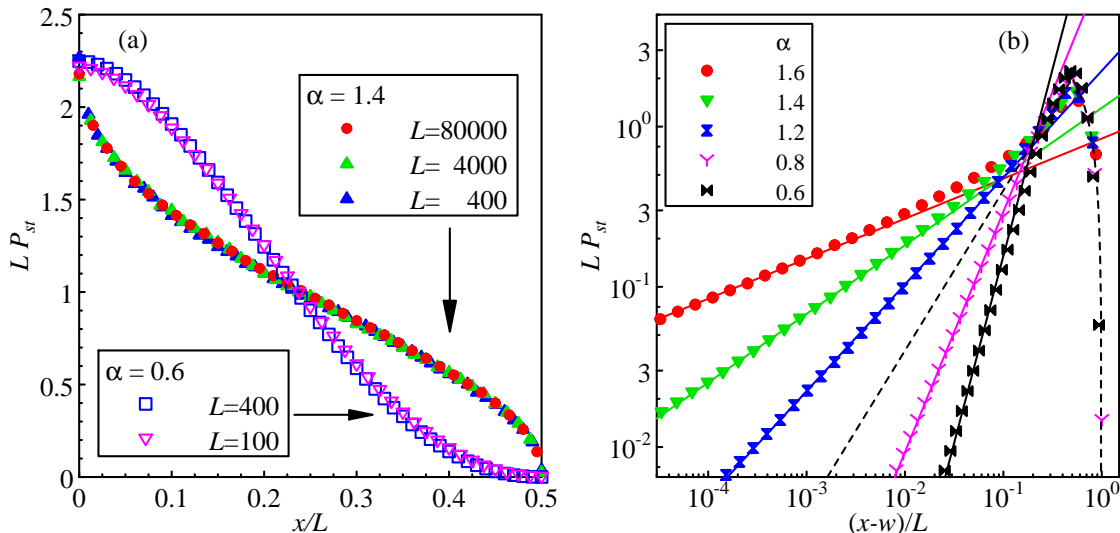


Figure 7. (a) Scaling plot of the stationary probability density for FBM on the interval $[-L/2, L/2]$ showing LP_{st} vs. x/L for $\alpha = 1.4$ and $\alpha = 0.6$ for several interval length L (only the right half of the interval is shown). Each distribution is based on 10^4 to 10^5 particles; P_{st} is averaged over a number of time steps after a stationary state has been reached. The simulation for $\alpha = 0.6$ and $L = 400$ required a maximum time of $t = 2^{27}$. (b) Scaled stationary probability density as function of the scaled distance $(x - w)/L$ from the absorbing wall located at $w = -L/2$ for several α . The solid lines are fits of the short distance behavior to the power law $P_{st} \sim (x - w)^\kappa$ with $\kappa = 2/\alpha - 1$. The dashed line shows the analytical result (17) for normal diffusion, without adjustable parameters. The statistical errors of the data are below one symbol size.

Nonetheless, $P_{st}(x)$ for $x \ll L$ can be fitted well with the expression $P_{st}(x) = a + b|x|^\kappa$ with the same exponent $\kappa = 2/\alpha - 1$ for all considered α .

Note that FBM on a finite interval with absorbing boundaries at both ends was studied perturbatively in Ref. [60], albeit without the particle source in the center of the interval.

6. Simulation results for the FLE with absorbing walls

Recent simulations have shown that FBM and the FLE behave in qualitatively different ways in the presence of *reflecting* walls. The probability distribution of FBM shows strong accumulation (for persistent noise) or depletion (for antipersistent noise) of particles close to the reflecting wall, both for semi-infinite intervals [42, 43] and for finite intervals [44, 45]. In contrast, the fractional Langevin equation on a finite interval with reflecting walls yields a flat stationary probability density, just like normal diffusion, for all α [46]. Some accumulation or depletion of particles (compared to normal diffusion) occurs on a semi-infinite interval. However, it is much less pronounced than in the FBM case. In the present section, we therefore compare and contrast the properties of the FLE with *absorbing* walls with the those found for FBM in Sec. 5.

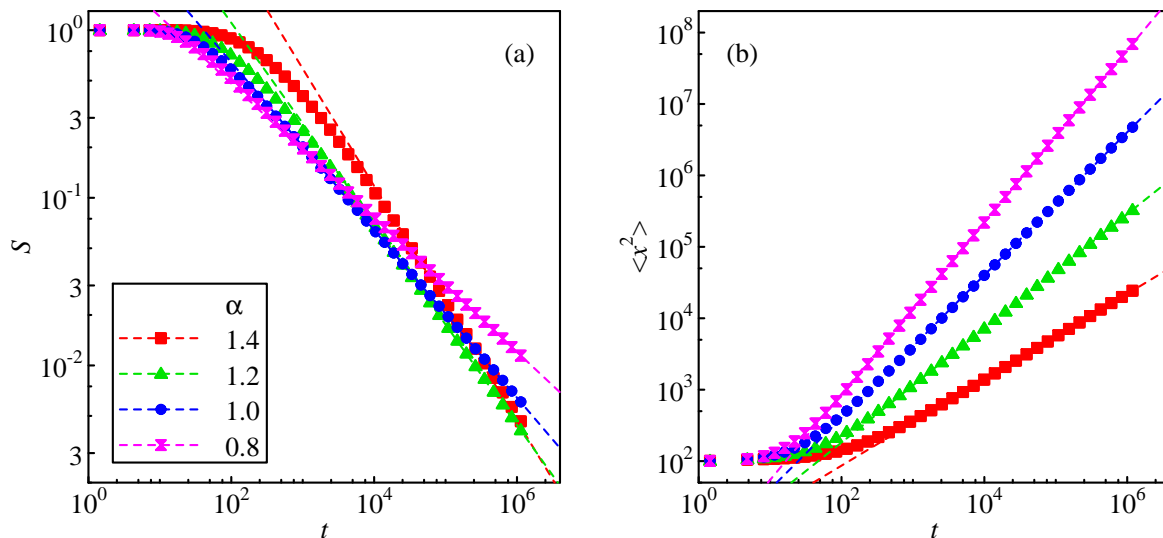


Figure 8. FLE on the semi-infinite interval $[0, \infty)$. (a) Survival probability S vs. time t for several values of α . The initial particle number is 4×10^6 , the time step $\epsilon = 0.08$, all particles start at $x_0 = 10$. The dashed lines are fits of the long-time behavior to the power law $S(t) \sim t^{-\alpha/2}$. (b) Mean square displacement $\langle x^2 \rangle$ of the surviving particles vs. time t for the same simulations as in panel (a). The dashed lines are fits of the long-time behavior to the power law $\langle x^2 \rangle \sim t^{2-\alpha}$. The statistical errors of all data points are smaller than the symbol size.

6.1. Semi-infinite interval

We start by considering the FLE on a semi-infinite interval $[0, \infty)$ with an absorbing wall at the origin. Particles start from rest at a position $x_0 > 0$ at time $t = 0$. Figure 8 presents the survival probability $S(t)$ and the mean-square displacement $\langle x^2 \rangle$ of the surviving particles for $x_0 = 10$ and several values of the exponent α that characterizes the covariance (6) of the random forces in the FLE. These correlations are persistent for $\alpha > 1$. Values $\alpha < 1$ correspond to antipersistent noise which can be included in our discretized FLE based on the discussion in Sec. 3.3.

Figure 8 resembles the corresponding Fig. 2 for FBM. The order of the curves is reversed, however, because persistent noise leads to subdiffusion for the FLE whereas antipersistent noise produces superdiffusion (the opposite behavior compared to FBM). Panel (a) demonstrates that the long-time decay of the survival probability follows the power-law $S(t) \sim t^{-\theta}$ with $\theta = \alpha/2$. The mean-square displacement from the origin for the surviving particles, shown in panel (b) follows the anomalous diffusion relation $\langle x^2 \rangle \sim t^{2-\alpha}$. Both power-law time dependencies agree with the corresponding FBM power laws if one replaces the FBM anomalous diffusion exponent α with its FLE counterpart $2 - \alpha$.

We now turn to the conditional probability density of the surviving particles, $P_s(x, t) = P(x, t)/S(t)$. The simulations confirm that P_s for the FLE fulfills the scaling

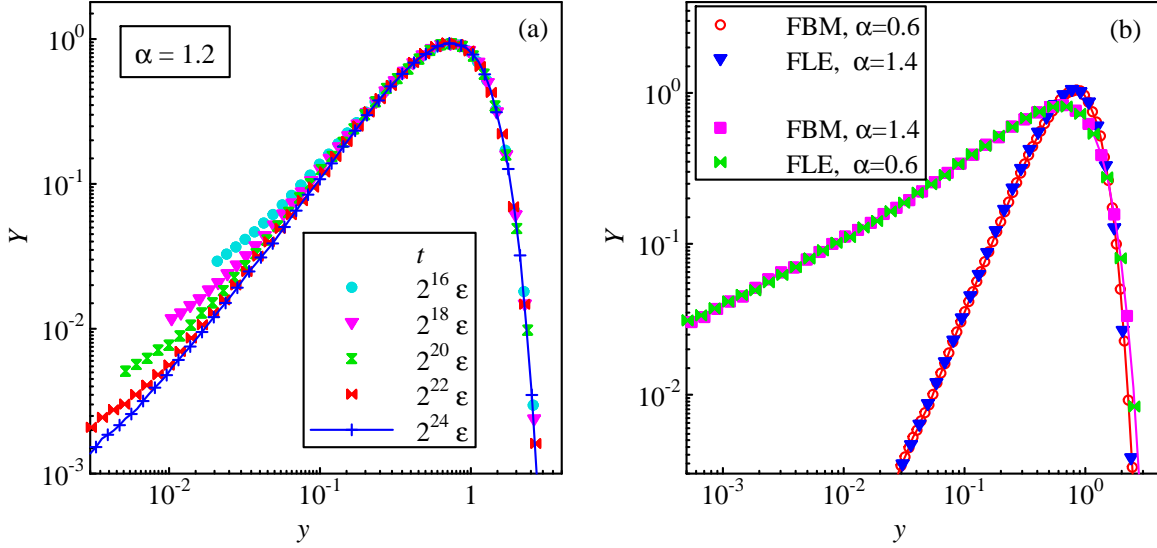


Figure 9. (a) Scaling plot of the conditional probability densities of the FLE on the interval $[0, \infty)$ at different times, expressed in terms of the variables $y = x/x_m(t)$ and $Y = P_s x_m(t)$ with $x_m(t) = \langle x^2(t) \rangle^{1/2}$. The time step is $\epsilon = 0.08$, and $\alpha = 1.2$. The initial particle number is 4×10^6 . P_s is averaged over a short time interval around the given time. (b) Comparison of the scaling functions $Y^{\text{fbm}}(y)$ for FBM and $Y^{\text{fle}}(y)$ for the FLE for two values of α . Data taken at time 2^{20} for FBM and $2^{24}\epsilon = 1\,342\,177$ for the FLE; the initial particle number is at least 4×10^6 . The statistical errors of the data points are about a symbol size or smaller.

form,

$$P_s(x, t) = \frac{1}{x_m(t)} Y_\alpha^{\text{fle}} \left[\frac{x}{x_m(t)} \right] \quad (23)$$

in the long-time limit $x_m(t) \gg x_0$. (Here, $x_m(t) = \langle x^2(t) \rangle^{1/2}$, as before.) Figure 9(a) demonstrates this for $\alpha = 1.2$. As was the case for FBM in Fig. 4(a), the data collapse is of good quality. Deviations of the small- x data from the common master curve can be attributed to finite-time discretization effects. They are suppressed with increasing t .

The scaling form (23) for the FLE is identical to the corresponding scaling form (18) for FBM. It is interesting to compare the scaling functions $Y_\alpha^{\text{fbm}}(y)$ for FBM and $Y_\alpha^{\text{fle}}(y)$ for the FLE. Figure 9(b) shows the scaled conditional probability densities for both FBM and the FLE for two values of α . (The data are taken at times $t > 10^6$ so that $x_m(t) \gg x_0$, and time discretization artifacts can be neglected for the positions considered.) Within our (small) statistical errors, the FBM and FLE scaling functions agree with each other if one replaces α by $2 - \alpha$,

$$Y_\alpha^{\text{fle}}(y) = Y_{2-\alpha}^{\text{fbm}}(y) . \quad (24)$$

This implies that the FLE scaling function is expected to follow the power law $Y_\alpha^{\text{fle}}(y) \sim y^\kappa$ with exponent $\kappa = \alpha/(2-\alpha)$ close to the absorbing wall, i.e. for $y \ll 1$. Our

numerical data can be fitted well with this power law all for all considered α (0.6, 0.8, 1.0, 1.2, and 1.4). For our most subdiffusive simulation, $\alpha = 1.4$, some slight deviations can be observed between this power law and the numerical data. As in the FBM case in Sec. 5.1, they can be attributed to the simulations not having progressed far enough into the asymptotic long-time regime.

6.2. Stationary state on finite interval

To overcome the numerical difficulties associated with the particle loss occurring in the simulations on the interval $[0, \infty)$ with an absorbing wall at the origin, we now consider the steady state of the FLE on the finite interval $[-L/2, L/2]$ with absorbing walls at both ends and a particle source in the center. This geometry is implemented analogously to the FBM case in Sec. 5.2. Particles start at the origin at $t = 0$. When a particle is absorbed by one of the walls, it is placed back at the origin. Unless noted otherwise, such a particle restarts from the origin with a fresh set of random forces and without memory of its velocities before the absorption event. For comparison, we also perform a number of calculations in which a particle retains the velocity memory and noise sequence from before the absorption event.

The time evolution of the mean-square displacement is shown in Fig. 10(a) for several values of the exponent α that characterizes the random force covariance (6). The figure shows that the mean-square displacement grows ballistically for a brief time initial period ($t \lesssim 5$), followed by anomalous diffusion governed by $\langle x^2 \rangle \sim t^{2-\alpha}$. After the particles reach the wall, $\langle x^2 \rangle$ approaches a constant value that varies with α , just as in the FBM case. The mean-square velocity $\langle v^2 \rangle$ quickly settles on a value very close to unity, in agreement with the fluctuation dissipation theorem. The slight deviation from unity (barely visible in the figure) can be attributed to the time discretization error, as discussed in Sec. 3.2.

Figure 10(b) shows how the stationary value of the scaled mean-square displacement $\langle x^2 \rangle / L^2$ depends on the exponent α , comparing our findings for the FLE with the FBM results of Sec. 5.2. The figure demonstrates that the stationary mean-square displacements of FBM and the FLE agree nearly perfectly, if one replaces α by $2 - \alpha$. This means that $\langle x^2 \rangle = L^2/24$ for normal diffusion, $\alpha = 1$ [see eq. (17)]. It also implies that $\langle x^2 \rangle$ approaches zero in most subdiffusive limit ($\alpha \rightarrow 2$ for the FLE), whereas it approaches the value $L^2/12$ in the ballistic limit ($\alpha \rightarrow 0$ in the FLE).

Let us now turn to the behavior of the stationary probability density $P_{st}(x, L)$ on the finite interval. By comparing the probability densities for several interval length L , we confirm that $P_{st}(x, L)$ fulfills the scaling form

$$P_{st}(x, L) = \frac{1}{L} Z_{\alpha}^{\text{fle}} \left(\frac{x}{L} \right), \quad (25)$$

where $Z_{\alpha}^{\text{fle}}(z)$ is a dimensionless scaling function, in analogy to eq. (22) for the FBM case. Figure 11(a) presents the corresponding scaling plots for two values of α . The figure also shows that the scaled probability density of FBM with exponent $2 - \alpha$ nearly

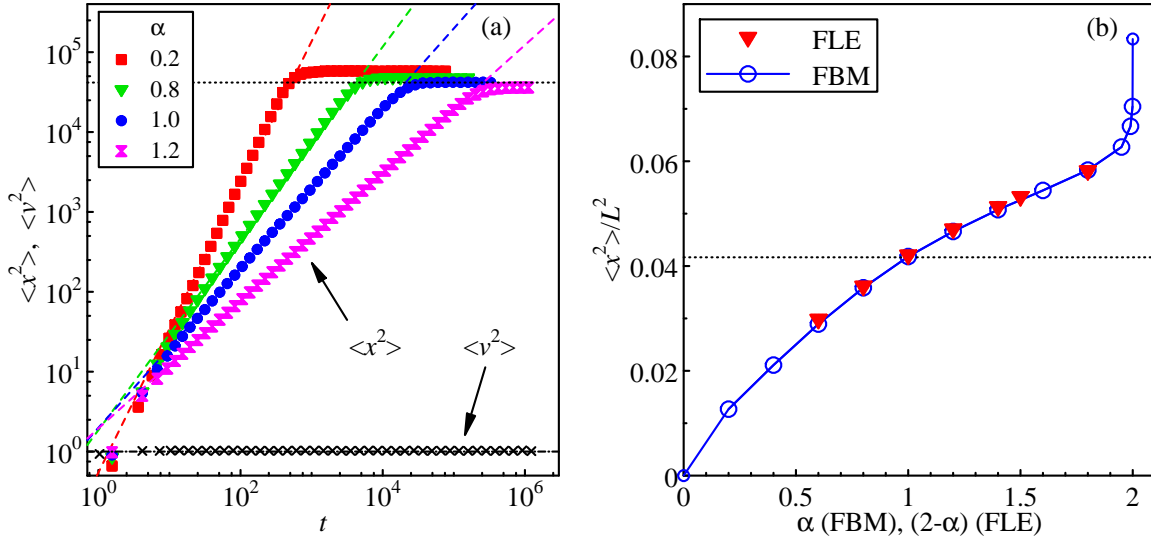


Figure 10. FLE on a finite interval $[-L/2, L/2]$ with absorbing walls at both ends and a source in the center. (a) Mean square displacement $\langle x^2 \rangle$ vs. time t for interval length $L = 1000$ and several α . The time step is $\epsilon = 0.04$, and the data are averages over 5×10^4 to 10^5 particles. The dashed lines are fits to the anomalous diffusion power law $\langle x^2 \rangle \sim t^{2-\alpha}$. The dotted line marks the stationary value $\langle x^2 \rangle = L^2/24$ for normal diffusion that follows from eq. (17). Also shown is $\langle v^2 \rangle$ for $\alpha = 1.2$. The dash-dotted line shows the expected value of unity. (b) Stationary value of $\langle x^2 \rangle / L^2$ vs. α or $2 - \alpha$, comparing the FLE results to the findings of Sec. 5.2 for FBM. The FLE data are based on interval length $L = 1000$ ($L = 200$ for $\alpha = 1.4$) and 5×10^4 to 10^5 particles. $\langle x^2 \rangle$ is averaged over a number of time steps after the stationary state is reached. The dotted line marks the stationary value $\langle x^2 \rangle = L^2/24$ for normal diffusion. All statistical errors are much smaller than the symbol size.

perfectly agrees with the scaled probability density of the FLE with exponent α . This implies that the scaling functions fulfill the relation

$$Z_{\alpha}^{\text{fle}}(z) = Z_{2-\alpha}^{\text{fbm}}(z). \quad (26)$$

In all FLE simulations on the finite interval reported so far, a particle absorbed by one of the walls restarts from the center with a fresh set of random forces and no memory of its velocities before the absorption event. To explore the effects of different restart conditions, we also perform a number of test calculations in which particles retain their velocity history and the random force sequence after an absorption event. A comparison of the stationary probability densities for the two restart conditions is presented in Fig. 11(b). As anticipated in Sec. 3.2, the stationary states for the two cases are not exactly identical (see the inset of the figure). The difference is easy to understand at a qualitative level. If a particle starts afresh with zero velocity, it will stay in the vicinity of the origin for a longer time, increasing the probability density in this region. This effect appears to increase with increasing α , perhaps because the damping kernel \mathcal{K}_{n-m} decays more slowly with time for larger α . However, the main panel of

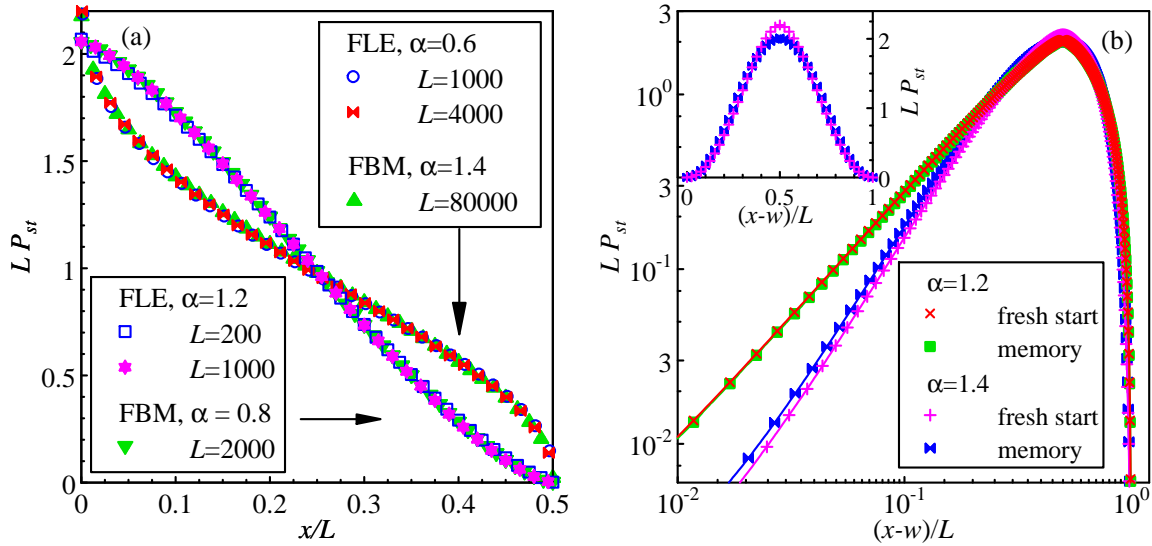


Figure 11. (a) Scaling plot of the stationary probability density for the FLE on the interval $[-L/2, L/2]$ showing LP_{st} vs. x/L for $\alpha = 1.2$ and $\alpha = 0.6$, $\epsilon = 0.04$, and several interval length L (only the right half of the interval is shown). Each distribution is based on 10^4 to 10^5 particles; P_{st} is averaged over a number of time steps after a stationary state has been reached. Also shown is the stationary probability density for FBM for $\alpha = 0.8$ and 1.4 . (b) Effect of the restart condition on the stationary probability density for $\alpha = 1.2$ ($L = 1000$) and $\alpha = 1.4$ ($L = 200$). The main panel shows LP_{st} vs. the scaled distance $(x - w)/L$ from the absorbing wall at $-L/2$. The inset shows the data for $\alpha = 1.4$ with linear axes. All statistical errors are much smaller than the symbol size.

Fig. 11(b) demonstrates that the functional form of the probability density close to the absorbing wall is not affected by the choice of restart condition. The curves for “fresh restarts” and “retained history” are parallel to each other for $x - w \ll L$, i.e., they follow the same power law but with slightly different prefactors.

To analyze the probability density close to the absorbing wall in more detail, we have therefore performed a set of simulations using the “retained history” restart condition. They are somewhat more efficient computationally because they do not require the recalculation of a full random number sequence after each absorption event. This allows us to reach up to 2^{29} time steps. Figure 12 presents the resulting stationary probability density in the wall region for several values of α . Sufficiently close to the absorbing wall, all distributions behave as powers of the distance $x - w$ (with $w = -L/2$) from the wall. In this regime, the data can be fitted with high accuracy with the expression $P_{st} \sim (x - w)^\kappa$ with $\kappa = \alpha/(2 - \alpha)$. (The exponent κ agrees with the FBM conjecture [48], $\kappa = 2/\alpha - 1$, if α is replaced by $2 - \alpha$, as was the case for the FLE on the semi-infinite interval.) For our most subdiffusive simulations, $\alpha = 1.4$ and 1.3 , slight deviations between the power law and the numerical data can be observed very close to the wall. They can be attributed to finite-size effects as the interval length we reach in these subdiffusive simulations are still only moderately large. In fact, the data can be

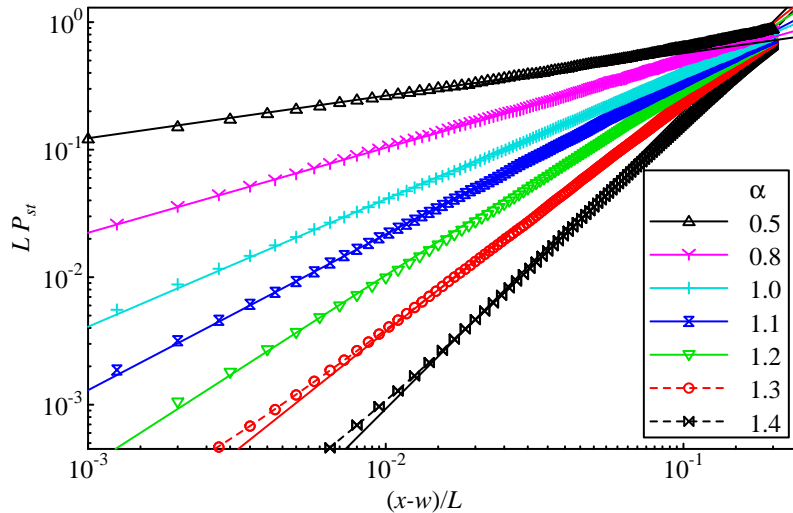


Figure 12. Scaled probability density LP_{st} vs. scaled distance from the wall $(x-w)/L$ for the FLE on the interval $[-L/2, L/2]$ with L ranging from 1000 for $\alpha = 1.4$ to 10^5 for $\alpha = 0.5$. Each simulation employs 5000 to 20000 particles that perform 2^{29} time steps of size $\epsilon = 0.08$ (2^{28} steps with $\epsilon = 0.04$ for $\alpha = 0.5$ and 0.8). P_{st} is averaged over a number of time steps after a stationary state has been reached. The solid lines represent fits of the probability density in the wall region $(x-w)/L \lesssim 0.03$ to the power law $P_{st} \sim (x-w)^\kappa$ with $\kappa = \alpha/(2-\alpha)$. The dashed lines for $\alpha = 0.6$ and 0.7 are fits with the function $P_{st} \sim (x-w+c)^\kappa$ which includes a subleading finite-size correction c . Statistical errors are much smaller than the symbol size.

fitted perfectly with the functional form $P_{st} \sim (x-w+c)^\kappa$ where the constant c acts as a subleading finite-size correction.

7. Conclusions

In summary, we have employed large-scale computer simulations to study and compare the probability density of FBM and the FLE in the presence of absorbing walls. We have considered two geometries, (i) the spreading for particles from a fixed starting point $x_0 > 0$ on the semi-infinite interval $[0, \infty)$ with an absorbing wall at the origin and (ii) the steady state on a finite interval with absorbing walls at both ends and a source in the center.

The FBM simulations on the semi-infinite interval agree with previous perturbative and numerical results in the literature [48–52, 61]. Specifically, the survival probability decays as $S(t) \sim t^{\alpha/2-1}$ for long times, $2Kt^\alpha \gg x_0^2$. In this limit, the conditional probability density for the surviving particles takes the scaling form $P_s(x, t) = Y_\alpha^{\text{fbm}}[x/x_m(t)]/x_m(t)$ where $x_m(t) \sim t^{\alpha/2}$ is the root mean-square displacement of the surviving particles. The dimensionless scaling function $Y_\alpha^{\text{fbm}}(y)$ vanishes as y^κ with $\kappa = 2/\alpha - 1$ close to the absorbing wall, i.e., for $y \ll 1$.

Interestingly, we have found the properties of the FLE on the semi-infinite interval to be identical to those of FBM if one replaces the FBM anomalous diffusion exponent

α by the anomalous diffusion exponent $2 - \alpha$ of the FLE. Specifically, the survival probability decays as $S(t) \sim t^{-\alpha/2}$ for long times whereas the root mean-square displacement of the surviving particles increases as $x_m(t) \sim t^{1-\alpha/2}$. Moreover, the entire scaling functions of the conditional probability densities for FBM and the FLE map onto each other under this replacement, $Y_\alpha^{\text{fle}}(y) = Y_{2-\alpha}^{\text{fbm}}(y)$. This implies that $Y_\alpha^{\text{fle}}(y)$ vanishes for $y \rightarrow 0$ as y^κ with $\kappa = \alpha/(2 - \alpha)$.

Our results for the steady state on the finite interval $[-L/2, L/2]$ paint a similar picture. The stationary probability density depends on α and fulfills the scaling form $P_{st}(x, L) = Z_\alpha^{\text{fbm}}(x/L) / L$ for FBM, and analogously for the FLE. Close to the absorbing walls at positions $w = \pm L/2$, the FBM scaling function behaves as $Z_\alpha^{\text{fbm}}(z) \sim |z \mp 1/2|^\kappa$, with the same exponent $\kappa = 2/\alpha - 1$ as for the semi-infinite interval. The behavior of the FLE in this geometry is identical to that of FBM after one replaces α by $2 - \alpha$. The scaling functions thus fulfill the relation $Z_\alpha^{\text{fle}}(z) = Z_{2-\alpha}^{\text{fbm}}(z)$, and $Z_\alpha^{\text{fle}}(z)$ vanishes with exponent $\kappa = \alpha/(2 - \alpha)$ close to $z = \pm 1/2$.

It is interesting to compare the effects of absorbing and reflecting boundaries on the probability density. For FBM, there is a clear analogy between the two cases. The probability density vanishes as $P \sim x^{2/\alpha-1}$ with distance x from an absorbing wall whereas it behaves as $P \sim x^{2/\alpha-2}$ close to a reflecting wall [42–45]. This means, for both boundary conditions, persistent noise increases the probability density close to the wall compared to normal diffusion. Anti-persistent noise, in contrast, reduces the probability density compared to normal diffusion.

For the FLE, such a clear analogy between absorbing and reflecting boundary conditions does not exist. The probability density of the FLE with absorbing walls can be mapped onto that of FBM with absorbing walls by replacing α with $2 - \alpha$, implying that the functional form of the probability density is strongly α dependent. In contrast, the stationary distribution of the FLE on a finite interval with reflecting walls is completely uniform independent of the value of α (as required in thermal equilibrium), and any accumulation and depletion effects for the FLE on a semi-infinite interval with a reflecting wall at the origin are much weaker than those of FBM [46].

What is the reason that FBM and the FLE behave very similarly for absorbing boundaries but in qualitatively different ways for reflecting boundaries? In the absorbing case, the particles do not actually “interact” with the boundary; whenever a particle crosses the boundary it is removed. This means that the free FBM or FLE trajectories completely determine the fate of a particle in the absorbing case. In the reflecting case, a particle stays in the system after reaching the wall, and its subsequent behavior depends on the wall interaction. For FBM, the (putative) displacements are determined by the noise and thus not affected by the wall. For the FLE, in contrast, the noise defines the forces while the displacements are determined by the instantaneous velocity which is affected by the wall.

We conclude by emphasizing that in many applications, perfectly absorbing or reflecting boundaries should be considered limiting cases, and the actual interaction of the trajectories with the confining walls may be more complicated. Moreover, the long-

range power-law correlations are often regularized beyond some time or length scale. To account for such a cutoff of the correlations, one can employ tempered fractional Gaussian noise [62]. Exploring these more complex situations remains a task for the future.

8. Acknowledgments

This work was supported in part by a Cottrell SEED award from Research Corporation and by the National Science Foundation under Grants No. DMR-1828489 and No. OAC-1919789. We thank R. Metzler for valuable discussions.

References

- [1] Einstein A 1956 *Investigations on the Theory of the Brownian Movement* (New York: Dover)
- [2] von Smoluchowski M 1918 Versuch einer mathematischen Theorie der Koagulationskinetik kolloider Lösungen *Z. Phys. Chem.* **92U** 129
- [3] Langevin P 1908 Sur la théorie du mouvement brownien *C. R. Acad. Sci. Paris* **146** 530–533
- [4] Hughes B 1995 *Random Walks and Random Environments, Volume 1: Random Walks* (Oxford: Oxford University Press)
- [5] Metzler R and Klafter J 2000 The random walk’s guide to anomalous diffusion: a fractional dynamics approach *Physics Reports* **339** 1 – 77
- [6] Höfling F and Franosch T 2013 Anomalous transport in the crowded world of biological cells *Rep. Progr. Phys.* **76** 046602
- [7] Bressloff P C and Newby J M 2013 Stochastic models of intracellular transport *Rev. Mod. Phys.* **85**(1) 135–196
- [8] Metzler R, Jeon J H, Cherstvy A G and Barkai E 2014 Anomalous diffusion models and their properties: non-stationarity, non-ergodicity, and ageing at the centenary of single particle tracking *Phys. Chem. Chem. Phys.* **16**(44) 24128–24164
- [9] Meroz Y and Sokolov I M 2015 A toolbox for determining subdiffusive mechanisms *Physics Reports* **573** 1 – 29 ISSN 0370-1573
- [10] Metzler R, Jeon J H and Cherstvy A 2016 Non-brownian diffusion in lipid membranes: Experiments and simulations *Biochimica et Biophysica Acta* **1858** 2451 – 2467 ISSN 0005-2736
- [11] Xie X S, Choi P J, Li G W, Lee N K and Lia G 2008 Single-molecule approach to molecular biology in living bacterial cells *Annual Review of Biophysics* **37** 417–444
- [12] Bräuchle C, Lamb D C and Michaelis J 2012 *Single Particle Tracking and Single Molecule Energy Transfer* (Weinheim: Wiley-VCH)
- [13] Manzo C and Garcia-Parajo M F 2015 A review of progress in single particle tracking: from methods to biophysical insights *Rep. Progr. Phys.* **78** 124601
- [14] Szymanski J and Weiss M 2009 Elucidating the origin of anomalous diffusion in crowded fluids *Phys. Rev. Lett.* **103**(3) 038102

- [15] Magdziarz M, Weron A, Burnecki K and Klafter J 2009 Fractional brownian motion versus the continuous-time random walk: A simple test for subdiffusive dynamics *Phys. Rev. Lett.* **103**(18) 180602
- [16] Weber S C, Spakowitz A J and Theriot J A 2010 Bacterial chromosomal loci move subdiffusively through a viscoelastic cytoplasm *Phys. Rev. Lett.* **104**(23) 238102
- [17] Jeon J H, Tejedor V, Burov S, Barkai E, Selhuber-Unkel C, Berg-Sørensen K, Oddershede L and Metzler R 2011 In vivo anomalous diffusion and weak ergodicity breaking of lipid granules *Phys. Rev. Lett.* **106**(4) 048103
- [18] Jeon J H, Monne H M S, Javanainen M and Metzler R 2012 Anomalous diffusion of phospholipids and cholesterol in a lipid bilayer and its origins *Phys. Rev. Lett.* **109**(18) 188103
- [19] Tabei S M A, Burov S, Kim H Y, Kuznetsov A, Huynh T, Jureller J, Philipson L H, Dinner A R and Scherer N F 2013 Intracellular transport of insulin granules is a subordinated random walk *Proc. Nat. Acad. Sci.* **110** 4911–4916 ISSN 0027-8424
- [20] Chakravarti N and Sebastian K 1997 Fractional brownian motion models for polymers *Chem. Phys. Lett.* **267** 9 – 13 ISSN 0009-2614
- [21] Panja D 2010 Generalized langevin equation formulation for anomalous polymer dynamics *J. Stat. Mech.* **2010** L02001
- [22] Mikosch T, Resnick S, Rootzen H and Stegeman A 2002 Is network traffic approximated by stable levy motion or fractional brownian motion? *Ann. Appl. Probab.* **12** 23–68
- [23] Janušonis S, Detering N, Metzler R and Vojta T 2020 Serotonergic axons as fractional brownian motion paths: Insights into the self-organization of regional densities *Front. Comp. Neuroscience* **14** 56 ISSN 1662-5188
- [24] Comte F and Renault E 1998 Long memory in continuous-time stochastic volatility models *Math. Financ.* **8** 291
- [25] Rostek S and Schöbel R 2013 A note on the use of fractional brownian motion for financial modeling *Econom. Model.* **30** 30 – 35 ISSN 0264-9993
- [26] Kolmogorov A N 1940 Wiener'sche spiralen und einige andere interessante kurven im hilbertschen raum *C. R. (Doklady) Acad. Sci. URSS (N.S.)* **26** 115–118
- [27] Mandelbrot B B and Ness J W V 1968 Fractional brownian motions, fractional noises and applications *SIAM Review* **10** 422–437
- [28] Kahane J P 1985 *Some Random Series of Functions* (London: Cambridge University Press)
- [29] Yaglom A M 1987 *Correlation Theory of Stationary and Related Random Functions* (Heidelberg: Springer)
- [30] Beran J 1994 *Statistics for Long-Memory Processes* (New York: Chapman & Hall)
- [31] Biagini F, Hu Y, Øksendal B and Zhang T 2008 *Stochastic Calculus for Fractional Brownian Motion and Applications* (Berlin: Springer)
- [32] Redner S 2001 *A guide to first-passage processes* (Cambridge: Cambridge University Press)
- [33] Hansen A, Engøy T and Måløy K J 1994 Measuring hurst exponents with the first return method *Fractals* **02** 527–533
- [34] Ding M and Yang W 1995 Distribution of the first return time in fractional brownian motion and its application to the study of on-off intermittency *Phys. Rev. E* **52**(1) 207–213

- [35] Krug J, Kallabis H, Majumdar S N, Cornell S J, Bray A J and Sire C 1997 Persistence exponents for fluctuating interfaces *Phys. Rev. E* **56**(3) 2702–2712
- [36] Molchan G M 1999 Maximum of a fractional brownian motion: Probabilities of small values *Commun. Math. Phys.* **205** 97–111
- [37] Jeon J H, Chechkin A V and Metzler R 2011 First passage behaviour of fractional brownian motion in two-dimensional wedge domains *EPL (Europhysics Letters)* **94** 20008
- [38] Aurzada F and Lifshits M A 2019 The first exit time of fractional brownian motion from a parabolic domain *Theory Probab. Appl.* **64** 490–497
- [39] Klimontovich Y L 1995 *Statistical theory of open systems - Volume 1: A unified approach to kinetic description of processes in active systems* (Dordrecht: Kluwer Academic Publishers)
- [40] Kubo R 1966 The fluctuation-dissipation theorem *Rep. Progr. Phys.* **29** 255–284
- [41] Lutz E 2001 Fractional langevin equation *Phys. Rev. E* **64**(5) 051106
- [42] Wada A H O and Vojta T 2018 Fractional brownian motion with a reflecting wall *Phys. Rev. E* **97**(2) 020102
- [43] Wada A H O, Warhover A and Vojta T 2019 Non-gaussian behavior of reflected fractional brownian motion *J. Stat. Mech.* **2019** 033209
- [44] Guggenberger T, Pagnini G, Vojta T and Metzler R 2019 Fractional brownian motion in a finite interval: correlations effect depletion or accretion zones of particles near boundaries *New J. Phys.* **21** 022002
- [45] Vojta T, Halladay S, Skinner S, Janušonis S, Guggenberger T and Metzler R 2020 Reflected fractional brownian motion in one and higher dimensions *Phys. Rev. E* **102**(3) 032108
- [46] Vojta T, Skinner S and Metzler R 2019 Probability density of the fractional langevin equation with reflecting walls *Phys. Rev. E* **100**(4) 042142
- [47] Chatelain C, Kantor Y and Kardar M 2008 Probability distributions for polymer translocation *Phys. Rev. E* **78**(2) 021129
- [48] Zoia A, Rosso A and Majumdar S N 2009 Asymptotic behavior of self-affine processes in semi-infinite domains *Phys. Rev. Lett.* **102**(12) 120602
- [49] Wiese K J, Majumdar S N and Rosso A 2011 Perturbation theory for fractional brownian motion in presence of absorbing boundaries *Phys. Rev. E* **83**(6) 061141
- [50] Delorme M and Wiese K J 2015 Maximum of a fractional brownian motion: Analytic results from perturbation theory *Phys. Rev. Lett.* **115**(21) 210601
- [51] Delorme M and Wiese K J 2016 Perturbative expansion for the maximum of fractional brownian motion *Phys. Rev. E* **94**(1) 012134
- [52] Arutkin M, Walter B and Wiese K J 2020 Extreme events for fractional brownian motion with drift: Theory and numerical validation *Phys. Rev. E* **102**(2) 022102
- [53] Qian H 2003 Fractional brownian motion and fractional gaussian noise *Processes with Long-Range Correlations: Theory and Applications* ed Rangarajan G and Ding M (Berlin, Heidelberg: Springer) pp 22–33 ISBN 978-3-540-44832-7
- [54] Makse H A, Havlin S, Schwartz M and Stanley H E 1996 Method for generating long-range correlations for large systems *Phys. Rev. E* **53**(5) 5445–5449
- [55] L’Ecuyer P 1999 Tables of maximally equidistributed combined lfsr generators *Math. Comput.* **68** 261–269 ISSN 0025-5718

- [56] Marsaglia G 2005 Double precision RNGs Posted to sci.math.num-analysis <http://sci.tech-archive.net/Archive/sci.math.num-analysis/2005-11/msg00352.html>
URL <http://sci.tech-archive.net/Archive/sci.math.num-analysis/2005-11/msg00352.html>
- [57] Zwanzig R 2001 *Nonequilibrium Statistical Mechanics* (Oxford: Oxford University Press)
- [58] Hänggi P 1978 Correlation functions and masterequations of generalized (non-markovian) langevin equations *Z. Phys. B* **31** 407–416 ISSN 1431-584X
- [59] Goychuk I 2012 *Viscoelastic Subdiffusion: Generalized Langevin Equation Approach* (John Wiley & Sons, Ltd) pp 187–253 ISBN 9781118197714
- [60] Wiese K J 2019 First passage in an interval for fractional brownian motion *Phys. Rev. E* **99**(3) 032106
- [61] Walter B and Wiese K J 2020 Sampling first-passage times of fractional brownian motion using adaptive bisections *Phys. Rev. E* **101**(4) 043312
- [62] Molina-Garcia D, Sandev T, Safdari H, Pagnini G, Chechkin A and Metzler R 2018 Crossover from anomalous to normal diffusion: truncated power-law noise correlations and applications to dynamics in lipid bilayers *New J. Phys.* **20** 103027